

RESEARCH ARTICLE

10.1029/2019JF005058

Key Points:

- Bedform amplitudes may decrease in the flow direction downstream of stable alluvial-bedrock transitions
- A stable pattern of downstream fining may form downstream of stable alluvial-bedrock transitions
- Surface-based bedload transport models reasonably capture bedload transport in bedrock reaches if the alluvial cover is accounted for

Supporting Information:

- Supporting Data S1
- Movie S1

Correspondence to:

S. Jafarinik,
jafarinm@email.sc.edu

Citation:

Jafarinik, S., Hernández Moreira, R., & Viparelli, E. (2019). Alluvial morphodynamics of bedrock reaches transporting, mixed-size sand. laboratory experiments. *Journal of Geophysical Research: Earth Surface*, 124, 3067–3089. <https://doi.org/10.1029/2019JF005058>

Received 5 MAR 2019

Accepted 12 NOV 2019

Accepted article online 15 NOV 2019

Published online 26 DEC 2019

Alluvial Morphodynamics of Bedrock Reaches Transporting Mixed-Size Sand. Laboratory Experiments

S. Jafarinik^{1,2} , R. Hernández Moreira², and E. Viparelli² 

¹European Centre Research and Teaching in Geosciences De L'envi, Aix-en-Provence, France, ²Department of Civil and Environmental Engineering, University of South Carolina, Columbia, SC, USA

Abstract Research on the morphodynamics of bedrock rivers has primarily focused on bedrock incision, and little is known about the alluvial morphodynamics of rivers with exposed bedrock surfaces. More specifically, there is a lack of information on the morphodynamics of low slope bedrock reaches due to the recent recognition of such systems. Here, we present the results of laboratory experiments specifically designed to gain novel insight into flow resistances, flow hydrodynamics, and sediment transport processes in equilibrium partially exposed bedrock reaches transporting nonuniform sand as bed material in low slope areas. The experiments show that (1) downstream of a stable alluvial-bedrock transition flow depth decreases in the streamwise direction, (2) bedform amplitude may decrease in the streamwise direction, and (3) stable patterns of downstream fining may form. Given the bedrock geometry, the water surface elevation at downstream boundary and the characteristics of the bedform regime in an alluvial channel subject to the same flow rate and sediment supply at equilibrium control bedform characteristics and sediment sorting patterns in the bedrock reach. When this distance is significantly smaller than the alluvial equilibrium flow depth or when the alluvial equilibrium bedform regime is close to the dune-antidune transition, bedforms in the bedrock reach are closer to the dune-antidune transition than at alluvial equilibrium with a consequent reduction in bedform amplitude. If the distance between the water level at the downstream boundary and the bedrock surface is close to the alluvial equilibrium flow depth and the alluvial equilibrium bedforms are well in the dune regime, a stable pattern of downstream fining can be expected. The comparisons between experimental and modeled sediment transport rates and equilibrium grain size distributions of the sediment further show that surface-based bedload transport models derived for alluvial systems reasonably predict equilibrium sediment transport rates and bed surface size distributions in bedrock reaches if the presence of exposed bedrock is accounted for in terms of alluvial cover fraction.

1. Introduction

Studies on the morphodynamics of bedrock and mixed bedrock-alluvial rivers have primarily focused on bedrock incision (e.g., Whipple et al., 2000; Whipple & Tucker, 2002; Whipple, 2004; Sklar & Dietrich, 2004; Turowski et al., 2007; Gasparini et al., 2007; Chatanantavet & Parker, 2008, 2009; Lamb et al., 2008; Lague, 2010, 2014; Hodge et al., 2011; Hodge et al., 2016; Chatanantavet et al., 2013; Johnson, 2014; Inoue et al., 2014; and Zhang et al., 2015), while the alluvial morphodynamics of bedrock rivers, which is important for, e.g., habitat preservation, restoration projects, and the performance of sediment budgets, has received less attention (Johnson & Whipple, 2007; Johnson & Whipple, 2010; Finnegan et al., 2007; Viparelli et al., 2015). Due to the paucity of field and laboratory data, and the lack of understanding of the interactions between sediment transport processes and the underlying bedrock surface (Carling et al., 2000; Carling, Golz, et al., 2000), few predictive models are available to estimate flow resistances and sediment fluxes in mixed alluvial-bedrock rivers. Very limited quantitative information is also available to account for the non-uniformity of the sediment size distribution in the presence of a bedrock surface (Hodge et al., 2011; Hodge et al., 2016). In the attempt to simplify the text, hereinafter “bedrock reach” is used to denote a mixed bedrock-alluvial reach as in Viparelli et al. (2015).

Carling et al. (Carling, Golz, et al., 2000; Carling et al., 2000) described isolated dunes in the German Rhine River migrating on top of an immobile layer of coarse gravel and noticed that the presence of dunes had an

impact on the flow resistances. Tuijnder et al. (2009) performed laboratory experiments on the equilibrium characteristics of supply limited dunes on an immobile gravel layer and found that dune height and wavelength increased with the average thickness of the fine sediment layer overlying the gravel substratum. These studies, however, did not propose predictive models to estimate flow resistances and bedform characteristics in reaches characterized by the interaction between bedrock or a gravel layer and the sediment transport.

Johnson (2014) noticed that to compute flow resistances in bedrock rivers transporting gravel as bed material, the different roughness between the areas covered with alluvium and areas with exposed bedrock should be accounted for. He thus introduced an *equivalent friction coefficient* defined as the average friction coefficient of the alluvial and the bedrock patches (Johnson, 2014). To extend Johnson's model to rivers with relatively mild slopes and bed material in the range of pea gravel and sand, the presence of bedforms such as dunes must be accounted for (Van Rijn, 1984).

To the authors' knowledge, Zhang et al. (2015) presented the first model of alluvial morphodynamics of bedrock rivers that accounts for the coevolution of alluvial and incisional processes. The key difference between the Zhang et al. (2015) formulation and previous models of bedrock river morphodynamics is in the calculation of the alluvial cover, i.e., the average areal fraction of the channel bed covered with alluvium, which controls bedrock incision and alluvial processes (Sklar & Dietrich, 2004). In particular, Zhang et al. expressed the alluvial cover as a function of the geometric characteristics of the bedrock surface and not as the ratio between sediment supply rate and sediment transport capacity (Sklar & Dietrich, 2004).

In recent years, bedrock reaches have been observed in low slope rivers such as lowermost Mississippi River and the distributary channels of the Wax Lake and Nile River deltas (Chen & Stanley, 1993; Nittrouer et al., 2011; Shaw et al., 2013). In addition, the presence of fixed (or semi fixed) layers in the Dutch Rhine River represents a challenge for river managers and engineers due to the lack of a theoretical framework for the alluvial morphodynamics of low slope rivers with a bedrock substrate (Sloff et al., 2012). In particular, there is a lack of predictive models to estimate flow resistances and sediment transport processes in these river reaches. These models, however, are necessary to adequately estimate water depths and sediment transport rates, adequately manage floods, guarantee safe navigation, and determine the feasibility of restoration projects.

For example, Viparelli et al. (2015) modified the Zhang et al. (2015) formulation to study the impacts of land-building engineered diversions on the lowermost Mississippi River, which is a low slope sand bed river with exposed bedrock and dune fields in the alluvial portion of the channel bed (e.g., Nittrouer et al., 2011). In particular, Viparelli et al. (2015) defined a minimum thickness of the alluvial cover for complete alluviation of the channel bed based on dune height during floods. In this way, they accounted for the geometric characteristics of the dune fields, which were hypothesized to have a significant influence on sand load calculations. They also did not need to specify the Zhang et al. (2015) macroroughness height for the bedrock surface, which could not be estimated from the available field data anyways. However, Viparelli et al. (2015) used a formulation to partition the flow resistances between skin friction and form drag derived for fully alluvial rivers (Wright & Parker, 2004) due to the lack of information on the influence of the bedrock surface on dune geometry. This formulation probably needs to be modified to account for (1) the interactions between the bedrock surface and the migrating bedforms in the form drag calculations and (2) the flow resistances associated with exposed bedrock (Johnson, 2014). In addition, Viparelli et al. (2015) showed that alluvial-bedrock and bedrock-alluvial transitions observed on the Mississippi River (Nittrouer et al., 2011) can be stable features of low slope bedrock rivers. In other words, in equilibrium condition, the location of the transition can be considered as fixed point that subtly moves in the upstream or downstream direction but remains confined within a relatively short reach.

Here, we present the results of laboratory experiments specifically designed to study the interaction between a nonerodible surface (the model bedrock) and sediment transport processes in terms of (1) bedform geometry, (2) longitudinal sediment sorting patterns, and (3) flow resistances. The experimental results provide novel insight on the physical processes that have to be accounted for in the formulation of predictive models of flow resistances and bed material transport of nonuniform bed material in low slope bedrock reaches.

The experiments were performed in a sediment feed flume and the analysis focused on equilibrium conditions, i.e., conditions in which the elevation of the alluvium averaged over a series of bedforms did not change in time (Anderson et al., 1975). Due to the limited length of the experimental facility, the experiments considered the case of bedload transport. In other words, the interaction between the suspended bed material load and the bedrock surface was out of the scope of the present study. The present experiments aimed to investigate how (1) flow resistances and grain size distribution of the bed surface changes with changes in alluvial cover fraction and (2) whether empirical relations used in fully alluvial reaches are able to predict the sediment load in mixed bedrock-alluvial reaches.

This paper is organized as follows: We first report background information on one-dimensional morphodynamic models of alluvial and bedrock rivers that is relevant to this study. We then describe the laboratory experiments and the relevant results. The spatial changes in flow resistance, bedload transport rates, grain size distribution of bed surface sediment, and bedform geometry are discussed and interpreted using models, procedures, and approaches developed to study the morphodynamics of fully alluvial rivers. This exercise shows that methods and procedures developed for fully alluvial rivers can be used to model the alluvial morphodynamics of bedrock systems if the presence of a nonerodible surface is explicitly accounted for in the calculations.

2. Background Information on 1D Models of Alluvial Morphodynamics Relevant to the Present Study

Here, we considered the case of a low slope river transporting sand and/or pea gravel, i.e., a system in which small-scale bedforms such as dunes are likely present. The problem is simplified with assumptions and approximations that are at the base of most one-dimensional models of river morphodynamics. Some of these assumptions can be easily relaxed for site specific applications (e.g., Viparelli et al., 2011, 2015).

The river reach is modeled as a sediment feed flume analog, i.e., water and sediment are fed from upstream at a specified rate and streamwise changes in flow discharge and sediment supply are not considered (Blom et al., 2016). The channel has a rectangular cross section of constant width. The exchange of sediment between the river channel and the floodplain is not accounted for. The slope of the bedrock surface, S_b , is assumed to be constant in space and time. We also assume:

1. Uniform bed material
2. Equal friction coefficient for the alluvial and the bedrock areas
3. No abrasion of gravel particles
4. Absence of subsidence, uplift, and sea level changes

Although Johnson (2014) recognized that the roughness of the bedrock surface likely influences the flow resistances in a bedrock reach, the assumption of equal friction coefficient for the alluvial and the bedrock areas (Zhang et al., 2015) is introduced because the roughness height of the bedrock surface is very difficult to quantify, likely varies from case to case, and may be larger or smaller than the roughness height of the alluvial patches. Thus, while the use of different friction coefficients for the bedrock and the alluvial areas seems to be reasonable, the implementation is problematic because proper values of roughness height for the bedrock and the alluvial areas cannot be determined. The experiments presented hereinafter provide novel and quantitative insight on how to quantify flow resistances in alluvial areas in presence of nonuniform bed material.

Let's consider a sediment feed flume with a model bedrock reach and no alluvial cover (Figure 1a). The elevation of the water level at the downstream boundary is ξ_d , and the elevation of the bedrock surface is denoted with $\eta_{b,x}$ where subscript x denotes that the elevation of the bedrock surface can vary in the streamwise direction. When water and sediment supply is turned on, an alluvial deposit with a downstream migrating front forms (Figure 1b). The front eventually reaches the downstream end of the flume, and, after sufficiently long time has elapsed, the system reaches a condition of equilibrium in which the average elevation of the alluvial deposit, $\eta_{a,x}$, the slope of the alluvial reach, and the water depth remain constant over time scales that are long compared to the time scales associated with bed material transport and bedform migration (Figure 1c) (Anderson et al., 1975; Parker, 2004).

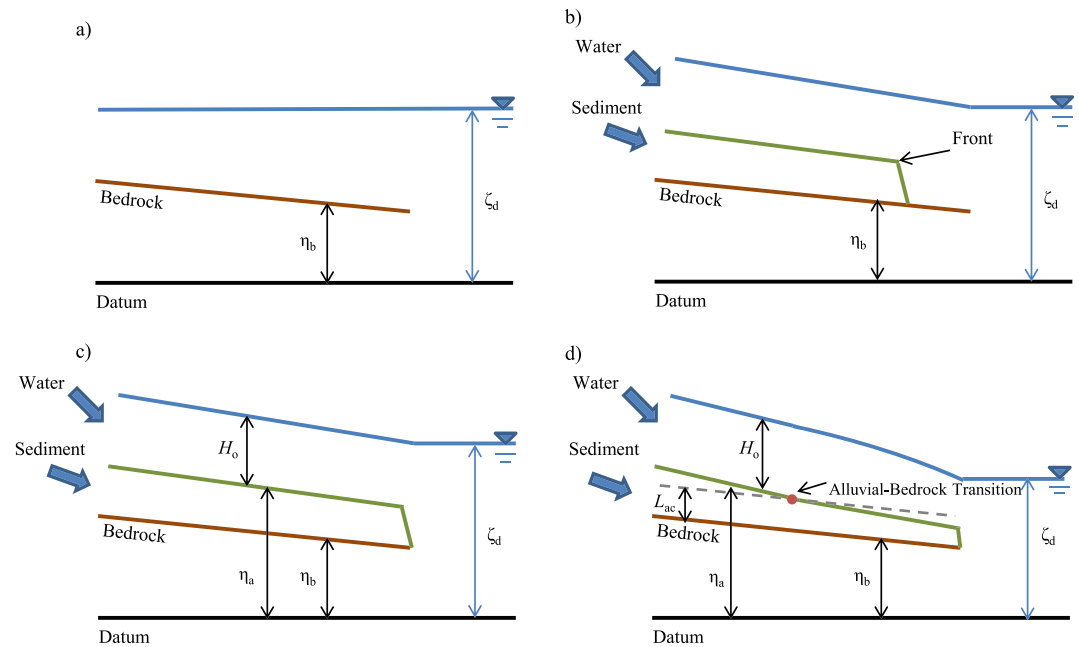


Figure 1. Schematic illustration of the evolution of an alluvial deposit in a sediment feed flume. (a) Empty flume with standing water, (b) alluvial deposit with a downstream migrating front, (c) alluvial equilibrium, and (d) equilibrium with an alluvial-bedrock transition. η_b represents the bedrock elevation, η_{bd} denotes the bedrock elevation at the downstream end of the channel, η is the alluvial bed surface elevation, H_o is the alluvial equilibrium water depth, ζ_d is the water level at the downstream end, and L_{ac} represents the minimum thickness of alluvial cover.

2.1. Alluvial Equilibrium

In alluvial rivers, the spatial and temporal evolution of an alluvial deposit is modeled with the Exner equation of conservation of bed material that, in a one-dimensional problem such as the experimental flume considered herein, takes the form:

$$(1-\lambda_p) \frac{\partial \eta_{a,x}}{\partial t} = -\frac{\partial q_{bm}}{\partial x}, \quad (1)$$

where λ_p denotes the bed porosity, t and x , respectively, are temporal and streamwise coordinates, and q_{bm} represents the volumetric bed material load per unit channel width, which is equal to the bed material transport capacity of the flow. It is important to note that q_{bm} represents temporal average over time scales that are long compared to the time scales characterizing bedform migration and bed material transport (Anderson et al., 1975). At equilibrium, the time rate of change of the deposit elevation $\eta_{a,x}$ is equal to zero. Thus, the bed material load is equal to the bed material transport capacity and to the bed material feed rate (equation 1).

The bed material transport capacity is generally computed with empirical relations linking q_{bm} to the Shields number τ^* , i.e., the nondimensional bed shear stress defined as $\tau_b/\rho RgD$, with τ_b denoting the bed shear stress, D the characteristic grain size of the bed material, ρ the water density, and R the submerged specific gravity of the bed material (Garcia, 2008). In particular, the bed material transport capacity is modeled with increasing functions of τ^* (Garcia, 2008). Recalling that at equilibrium q_{bm} does not change in space and time, the equilibrium bed shear stress τ_b has to be constant in the streamwise direction and in time. In other words, at alluvial equilibrium, the flow can be modeled as steady and uniform over time scales that are long compared to the time scales of bedform migration (Anderson et al., 1975; Parker, 2004).

2.2. Equilibrium with a Stable Alluvial-Bedrock Transition

When ζ_d is sufficiently small, the river reaches equilibrium conditions with exposed bedrock and steady but nonuniform flow (Viparelli et al., 2015) (Figure 1d). Here, we follow Viparelli et al. (2015), and we introduce

the minimum thickness of alluvial cover for complete alluviation of the channel bed, L_{ac} . L_{ac} represents the minimum thickness of the alluvial layer such that the presence of the bedrock surface with its irregularities (roughness) does not influence in-channel sediment transport processes. It follows that $\eta_{b,x} + L_{ac}$ represents the minimum elevation of the alluvial deposit for complete alluviation of the channel bed. When $\eta_{a,x} > \eta_{b,x} + L_{ac}$, the reach is defined to be alluvial, while for $\eta_{a,x} < \eta_{b,x} + L_{ac}$, the reach is defined to be bedrock. In this formulation, an alluvial-bedrock or a bedrock-alluvial transition occurs when $\eta_{a,x} = \eta_{b,x} + L_{ac}$ (Figure 1d).

If ξ_d is greater than the sum of H_o , L_{ac} , and $\eta_{b,d}$, with H_o denoting the alluvial equilibrium flow depth and $\eta_{b,d}$ the elevation of the bedrock surface at the downstream end of the flume, conditions of alluvial equilibrium can be obtained. Conversely, when $\xi_d < H_o + L_{ac} + \eta_{b,d}$, exposed bedrock may characterize the equilibrium configuration of the considered reach. In particular, if the slope of the bedrock surface S_b is smaller than the slope of an alluvial equilibrium reach subject to the same flow rate and sediment supply of the bedrock reach, S_o , a stable alluvial-bedrock transition can form as illustrated in Figure 1d (Viparelli et al., 2015).

In the alluvial reach of Figure 1d, the equilibrium bed slope is equal to S_o , the equilibrium flow depth is equal to H_o , and the equilibrium bed material load is equal to the bed material transport capacity and to the feed rate. In the bedrock reach of Figure 1d, the limited space between the fixed downstream water level and the bedrock surface forces the equilibrium flow depth to decrease, i.e., downstream of a stable alluvial-bedrock transition the flow accelerates in the flow direction (Viparelli et al., 2015).

Recalling that the bed shear stress $\tau_b = \rho C_f U^2$ (Parker, 2004), it immediately follows that if the dimensionless friction coefficient, C_f , is assumed to be the same in the alluvial and in the bedrock reaches (assumption 2), and the mean flow velocity, U , increases in the flow direction, the bed shear stress and the bed material transport capacity also increase in the streamwise direction. At equilibrium, however, the bed material load must be equal to the feed rate to satisfy sediment mass balance, and thus the bed material load in the bedrock reach should be smaller than the transport capacity in order to avoid deposition there.

Bedload transport in bedrock reaches is generally modeled as the product of the bed material transport capacity q_c and the alluvial cover p_c , i.e., $q_{bm} = p_c q_c$ (Sklar & Dietrich, 2004; Zhang et al., 2015) where p_c is the aerial fraction of the bed surface covered with alluvial material, so that in a fully alluvial reach $p_c = 1$ and in a bedrock reach $p_c < 1$. Thus, the streamwise increasing bed material transport capacity downstream of a stable alluvial-bedrock transition should be balanced by p_c decreasing in the flow direction (Viparelli et al., 2015).

Subsidence, uplift, and changes in water level at the downstream boundary (assumption 4) result in a change in distance between water level at the downstream boundary and the bedrock surface. If this distance increases (subsidence and base level rise), the alluvial-bedrock transition will migrate downstream. Conversely, it is reasonable to expect an upstream migration of the alluvial-bedrock transition in the case of base level fall and uplift.

The experiments presented in the following sections were specifically designed to explore how assumptions (1) and (2), i.e., uniform bed material and equal friction coefficient for the alluvial and the bedrock areas, can be relaxed. In particular, the objectives of the experiments were (1) observe the formation of a stable alluvial-bedrock transition in laboratory experiments, (2) characterize flow conditions upstream and downstream of a stable alluvial-bedrock transition, (3) determine if bedload transport relations for nonuniform bed material can be used to predict sediment fluxes in bedrock reaches, (4) compare bedform geometry in alluvial and bedrock reaches, and (5) characterize equilibrium sediment sorting patterns in the bedrock reach.

3. Overview on the Experiments

We performed the experiments in the 13 m long, 0.50 m wide, and 0.9 m deep horizontal sediment feed flume in the Hydraulics Laboratory of Civil and Environmental Engineering Department at the University of South Carolina schematically represented in Figure 2. A 6 m long and 0.19 m wide test reach was built with marine plywood to perform experiments on bedload transport. The entire flume length could not be used because the downstream most possible location for the sediment trap was at 8.5 m from the flume entrance. The cross section in the upstream part of the flume was gradually narrowed from 0.5 m to 0.19 m to reduce the likelihood of having three-dimensional bedforms and to limit the volume of

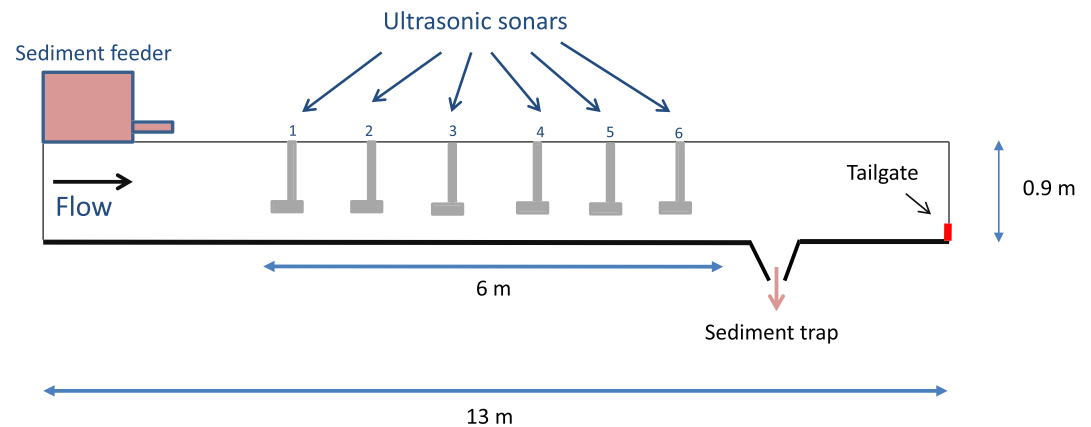


Figure 2. Schematic representation of the experimental apparatus. Drawing not to scale.

sediment used in the experiments. This gradual reduction of the cross section occupied the first 2.5 m of the flume, leaving a 6 m long test reach.

The downstream water level was controlled with a tailgate. The constant flow rate was supplied from the head tank of the laboratory and measured with a calibrated orifice plate. The model bedrock surface was a horizontal ($S_b = 0$) sheet of white plywood glued on to the bottom of the flume. Details on the experimental facility are available through the wiki page of the Sediment Experimentalists Network (<http://sedexp.net/content/university-south-carolina-columbia-hydraulics-laboratory>).

The experiments were performed with two types of sand: uniform sand with geometric mean diameter $D_g = 1.11$ mm and geometric standard deviation $\sigma_g = 1.44$ and nonuniform sand with $D_g = 0.87$ mm, and $\sigma_g = 1.69$. The D_g of the nonuniform sand was finer than the D_g of the uniform material, and this might have had a subtle impact on the comparison between experiments performed with uniform and nonuniform materials. The grain size distribution of the sand used in the experiments is presented in Figure 3. These

materials were chosen to prevent suspended sediment transport and the formation of small-scale ripples.

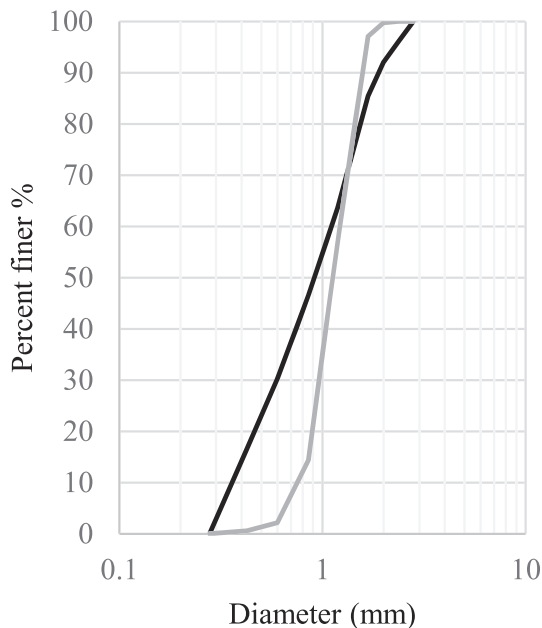


Figure 3. Grain size distribution of the material used in the experiments. The gray line is the uniform material used in Runs 1 and Runs 2. The black line represents the nonuniform material used in Runs 3–8.

We designed four groups of paired experimental runs (Run 1–8) summarized in Table 1 in terms of flow and sediment feed rates, distance between the water level at the downstream boundary and the bedrock ξ_d , alluvial equilibrium flow depth H_o , and sand type. Each pair of runs had the same flow rate, feed rate, and sediment type but differed for the water level at the downstream boundary, which dictated if mobile bed equilibrium was either fully alluvial or was characterized by a stable alluvial-bedrock transition. In the last column of Table 1, we report whether the equilibrium was fully alluvial or had exposed bedrock.

The initial conditions of the experimental runs varied from one run to the other. The fully alluvial runs commenced with no alluvial deposit (Figure 1a). Some of the runs with an equilibrium bedrock reach commenced with the alluvial equilibrium deposit obtained for the same flow and sediment feed rates (Figure 1c); others commenced with an empty flume. In the runs with an initial alluvial deposit, the water level at the downstream boundary was gradually lowered to obtain a stable alluvial-bedrock transition at approximately 2 m from the flume entrance (Figure 1d), as further discussed in the result section. Note that equilibrium conditions in a sediment feed flume are not dependent on the initial conditions (Parker & Wilcock, 1993), which therefore did not influence the results presented below (see Supporting Material of Viparelli et al., 2015).

Table 1
Experimental Conditions

Run	Flow rate (L/s)	Feed rate (gr/min)	ξ_d (m)	H_0	Grain size	Condition
1	20	700	0.224	0.176	Uniform	Fully alluvial
2	20	700	0.160		Uniform	Exposed bedrock
3	20	700	0.223	0.172	Nonuniform	Fully alluvial
4	20	700	0.154		Nonuniform	Exposed bedrock
5	20	400	0.225	0.186	Nonuniform	Fully alluvial
6	20	400	0.186		Nonuniform	Exposed bedrock
7	10	400	0.146	0.086	Nonuniform	Fully alluvial
8	10	400	0.083		Nonuniform	Exposed bedrock

Note. ξ_d denotes the vertical distance between the bedrock surface and the water level at the downstream boundary. H_0 is the alluvial equilibrium flow depth.

It is important to note here, however, that in the case of a relatively steep bedrock surfaces (slope $> \sim 0.005$ in the experiments by Chatanantavet & Parker, 2008), equilibrium conditions may depend on the presence of initial alluvial patches or of a sufficiently thick layer of alluvium (Chatanantavet & Parker, 2008). The bedrock slopes considered in this experimental study are comparable to the slopes of lowland sand bed rivers (10^{-4} or less). For example, the bedrock slope in the mixed alluvial-bedrock Mississippi River is 7×10^{-6} in the New Orleans area and 1.2×10^{-4} approximately 100 river kilometers upstream of the Gulf of Mexico (Viparelli et al., 2015 and references therein). These slopes are at least one order of magnitude milder than the slopes considered by Chatanantavet and Parker (2008), and equilibrium conditions on relatively mild bedrock slopes are not dependent on the initial alluvial cover of the model bedrock surface (Chatanantavet & Parker, 2008). If steep bedrock surfaces (slopes with order of magnitude equal or larger than 10^{-3}) are considered in a morphodynamic model, the Viparelli et al. (2015) model should be adequately modified to account for the different roughness between the bedrock surface and the alluvial areas.

3.1. Experimental Procedure

During each run, 20 min long series of water surface elevation measurements were recorded every hour with Baumer sonar probes at 0.2 m, 1.9 m, 3.9 m, and 5.95 m from the test reach entrance. The average water surface elevation was then calculated at each location. When the percent error between two consecutive water surface elevation measurements at the same location became smaller than 5%, we assumed that the system reached conditions of equilibrium. Depending on the experimental conditions, i.e., feed rate, flow rate, and water level at the downstream boundary, it took between 4 and 10 hours to reach conditions of equilibrium.

At equilibrium, 20 min long series of water surface elevation measurements were recorded at eight locations, i.e., 0 m, 0.3 m, 1 m, 2 m, 3 m, 4 m, 5 m, and 6 m from the test reach entrance, and 30 min long series of bed elevation measurements were recorded with a JSR ultrasonic sonar pulser (Wong et al., 2007) at 16 locations, i.e., 0.21 m, 0.51 m, 0.81 m, 1.21 m, 1.51 m, 1.81 m, 2.21 m, 2.51 m, 2.81 m, 3.21 m, 3.51 m, 3.81 m, 4.81 m, 5.21 m, 5.51 m, and 5.81 m from the test reach entrance, to determine the average bed elevation and characterize bedform geometry and alluvial cover fraction. Then the experiment terminated.

To ensure that the duration of bed and water measurements is representative of average conditions over time scales much longer than the time scales of bedform migration, we measured water and bed surface elevation for different durations. The results of this exercise for Run 5 (400 gr/min of feed rate and 20 l/s of flow rate) are presented in Table 2 in terms of mean and standard deviation of the measured water surface elevations (columns 2 and 4). The Baumer probe was located 5 m downstream of the test reach entrance. The mean water surface elevation (column 2) represents the temporal average of the measurements, and it is the quantity to be used in the one-dimensional morphodynamic framework presented in section 2. The standard deviation of water surface elevation is a measure of the variability of the instantaneous water surface elevation around the mean caused by the interactions between the migrating bedforms and the free surface flow (Engelund & Hansen, 1967).

Table 2
Mean Water Surface Elevation and Standard Deviation of the Water Surface Elevation for Different Measurement Durations in Run 5 at 5 m From the Test Reach Entrance

Time (min)	Mean water depth		Standard deviation	
	Value (cm)	Error %	Value (cm)	Error %
5	21.8	0.1	0.28	34.6
10	22.0	0.7	0.35	19.9
15	22.0	0.9	0.36	17.5
20	21.8	0.2	0.44	0.8
25	21.8		0.43	

We measured 5, 10, 15, 20, and 25 min long series of water surface elevation. Based on similar experiments performed in the same flume with the same material (Hernandez Moreira, 2016), we assumed that the 25 min long measurements were representative of the flow conditions averaged over a series of bedforms. We then computed the percent error for the mean (Table 2, column 3) and the standard deviation (Table 2, column 5) of water surface elevation for the 5, 10, 15, and 20 min long measurements as $|v_i - v_{25}| \cdot 100 / v_{25}$, where v_{25} denotes the value of the 25 minute long measurement and v_i is the value of the short measurements, with the subscript i denoting different measurement durations. After 20 min of measurement time, the errors did not exceed 1%, i.e., 20 min was a sufficiently long measurement time to reasonably determine the water surface elevation averaged over a series of bedforms. The same procedure was repeated for the bed elevation measurements, and a duration of 30 min was found to be appropriate to compute the bed elevation averaged over a series of bedforms and the average characteristics of the channel bed.

At the end of each experiment, we took pictures of the bed surface, and we then sampled the entire deposit surface to characterize the spatial changes in grain size distribution of the surface sediment. Each sample was 25 cm long and 19 cm wide and was collected by siphoning the bed surface sediment. The definition of bed surface in presence of bedforms is not straightforward. It can be defined as the 1–3 grain diameters thick layer of the bedforms stoss face (Blom et al., 2006), or it can be described as the bed layer with moving bedforms (Viparelli et al., 2013). In this study we used the latter definition because it was practically impossible to define a 1–3 diameter thick layer in the runs with exposed bedrock where portions of the channel bed were not entirely covered with alluvium. In other words, in the bedrock reaches, we assumed that the entire deposit represented the bed surface. Each sediment sample was dried in an oven, and then the grain size distribution was measured with sieve analysis.

3.2. Calculation of the Flow Characteristics at Equilibrium

Equilibrium flow depths and velocities were determined from the measurements of water surface and bed elevation. Because water surface and bed elevation were measured in different locations, water surface elevation measurements were linearly interpolated to compute the flow depth spatial distribution $H(x)$ as the difference between the (interpolated) average water surface elevation and the measured bed elevations. The flow velocity $U(x)$ was then estimated as the ratio between the flow discharge and the cross-sectional area.

4. Results

The experimental results are presented in two sections: *alluvial equilibrium* and *equilibrium with exposed bedrock*. Equilibrium conditions are described in terms of streamwise changes in standard deviation of the time series of bed elevation, water depth, and geometric mean grain size of the bed surface sediment. Measurements of water surface elevation and slope allowed us to characterize the spatial changes in flow velocity and resistance at equilibrium.

At equilibrium, the standard deviation of the time series of bed elevation σ_η is a measure of the variability of the bed elevation around its mean value, which is constant in time. In the case of equilibrium under lower regime, i.e., plane bed condition (no bedforms), σ_η increases with increasing bed shear stress (Wong et al., 2007). Here, we use σ_η to quantify the variability of bed elevation associated with bedload transport and downstream migrating bedforms.

The time series of bed elevation presented in Figure 4a was recorded at equilibrium during Run 3. Two types of bed elevation changes can be identified, small amplitude, high frequency changes associated with bedload transport (Wong et al., 2007) and high amplitude, low frequency changes associated with downstream migrating bedforms. Figure 4a clearly shows that the magnitude of the bed elevation changes associated with bedform migration is orders of magnitude larger than the magnitude of the bed elevation changes associated with bedload transport. A close look at Figure 4 also shows that one bedform is different from the other. In other words, relatively small and large bedforms are randomly spread throughout the time series. We are interested in the calculations of flow resistances and sediment fluxes averaged over a series of bedforms Anderson et al., 1975 to quantify the equilibrium form drag. We thus used the standard deviation of bed elevation (σ_η) to characterize the average bedform amplitude: σ_η is largest in the experimental runs with largest bedforms. The green lines in Figure 4 are drawn σ_η and $2\sigma_\eta$ from the average bed elevation showing that $4\sigma_\eta$

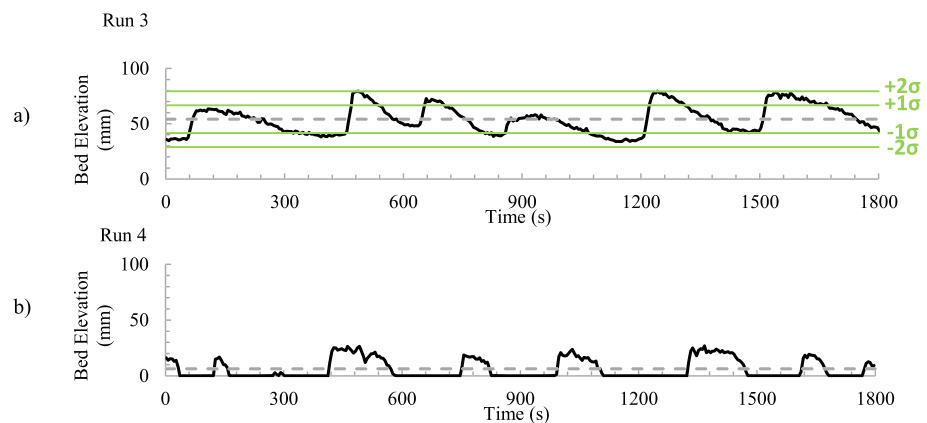


Figure 4. Time series of bed elevation fluctuations (a) Run 3 (700 g/min, 20 l/s, nonuniform material, alluvial run) at 5.21 m from the test reach entrance. (b) Run 4 (700 g/min, 20 l/s, nonuniform material, equilibrium with exposed bedrock) at 5.21 m from the test reach entrance. The dashed gray line indicates average bed elevation, and the green lines represent one and two standard deviation (σ_η) of the bed elevation fluctuation above and below the average bed elevation.

is a reasonable measure for the height of the large bedform and $2\sigma_\eta$ is a reasonable measure of the small bedform height. Further, if the probability density function of bed elevations is approximated with a Gaussian distribution (Singh et al., 2011), more than 96% of the changes in bed elevation are contained in an interval $2\sigma_\eta$ around the mean.

In previous studies of bedrock river morphodynamics, the alluvial cover fraction was defined as the aerial fraction of the bed covered with alluvium (Hodge et al., 2011; Inoue et al., 2014; Johnson, 2014). Due to the lack of sufficiently long time series of bed surface pictures, we defined the alluvial cover fraction based on the time series of bed elevation. A time series of equilibrium bed elevation in a bedrock reach for Run 4 is presented in Figure 4b. The high values of bed elevation correspond to periods in which the bed was covered with alluvium, and the nearly constant low values of bed elevation identify periods of time in which the model bedrock was exposed. We thus defined the alluvial cover fraction as the average fraction of time in which the model bedrock was covered with alluvium. Given the very limited lateral changes in bedform shape within the 19 cm wide cross section, we assumed that the point measurement of alluvial cover fraction was representative of the entire cross section. Video s1 in the Supplementary Information shows a side view of the flume in a mixed bedrock-alluvial reach during Run 4 and confirms that the lateral changes in bedform geometry can be reasonably considered negligible.

4.1. Alluvial Equilibrium

The results of the alluvial equilibrium runs are presented in Figure 5 in terms of streamwise changes in (1) standard deviation of bed elevation σ_η (a, c, f, and i), (2) average water depth H (b, d, g, and j), and (3) geometric mean diameter of the bed surface sediment, D_{sg} (e, h, and k). The results of the run with uniform sand, flow rate equal to 20 l/s, and feed rate equal to 700 g/min (Run 1) are presented in panels a and b. The results of the runs with nonuniform sand are in panels c–k. The results of Run 3, which had the same flow rate and feed rate of Run 1, are in panels c–e. Panels e–g summarize the results of the alluvial equilibrium run with flow rate equal to 20 l/s and feed rate equal to 400 g/min (Run 5); and panels i–k report the results of the alluvial equilibrium with flow rate equal to 10 l/s and feed rate equal to 400 g/min (Run 7).

The values of σ_η reveal that the equilibrium bedform amplitude was not constant in the streamwise direction, as indicated with the red ovals in Figure 5 (a, c, f, and i). In the upstream part of the test reach, the bed was covered with relatively small bedforms that grew as they moved in the streamwise direction until their heights and wavelengths became uniform for the rest of the flume length. The streamwise changes in equilibrium bedform height are shown in Figure 6 for Run 3, in terms of time series of bed elevation measurements (black lines). A time series collected in the upstream part of the test reach (1.81 m from the test reach entrance) is presented in Figure 6a, and a series collected in the downstream part of the flume

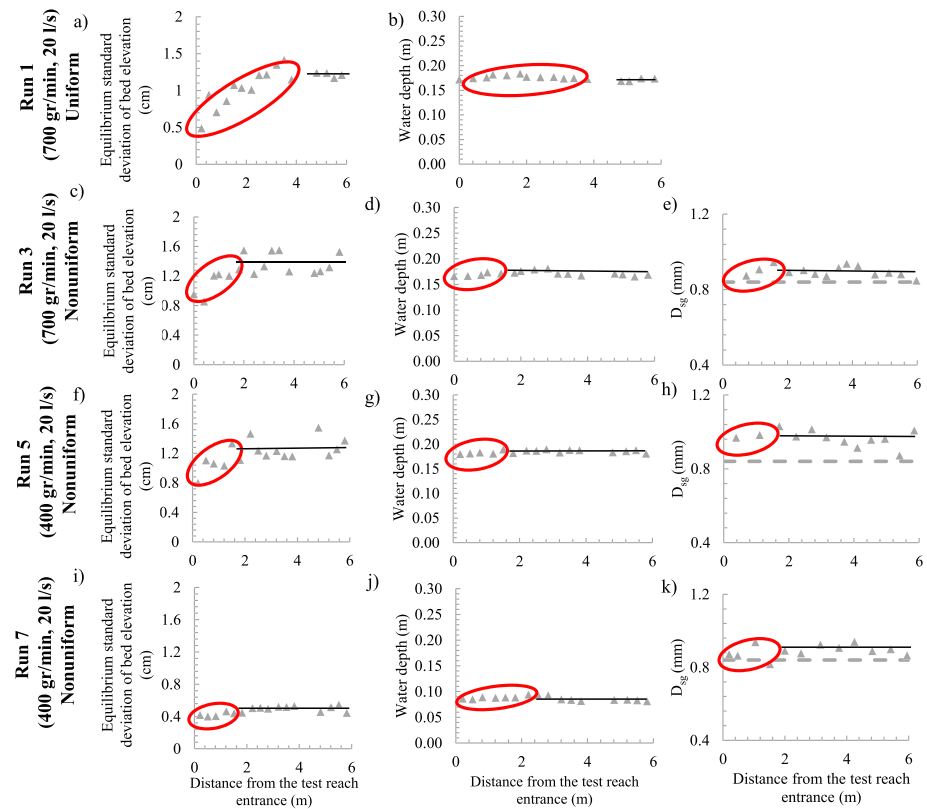


Figure 5. Spatial changes in equilibrium standard deviation of the bed elevation, σ_η , water depth, H , and geometric mean diameter of the surface sediment, D_{sg} , in the fully alluvial runs (Runs 1, 3, 5, and 7). Symbols represent the experimental points. The black lines are the regression lines through the experimental points. The dashed gray line in the D_{sg} plots represents the geometric mean size of the sediment feed. Red ovals qualitatively indicate the bedform development region.

(5.21 m from the test reach entrance) is in Figure 6b. The comparison between panels a and b clearly shows that the bedform height in the upstream part of the flume was smaller than in the downstream reach.

The region of the test reach in which the bedform amplitude grew in the streamwise direction is here called *bedform development region*, and it is indicated with ovals in Figure 5. It is interesting to note that in the runs with nonuniform sediment (Figure 5c, 5f, and 5i), the bedform development region was ~ 2 m long, while in

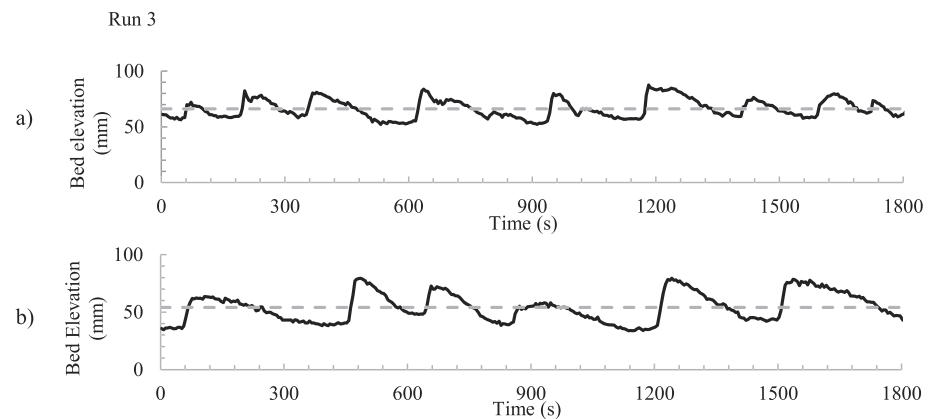


Figure 6. Time series of the bed elevation fluctuations in Run 3 (700 g/min, 20 l/s, nonuniform material, alluvial equilibrium). (a) Measurements at 1.81 m from the test reach entrance. (b) Measurements at 5.21 m from the test reach entrance. The solid lines are the sonar measurements, and the dashed gray line is the time averaged bed elevation.

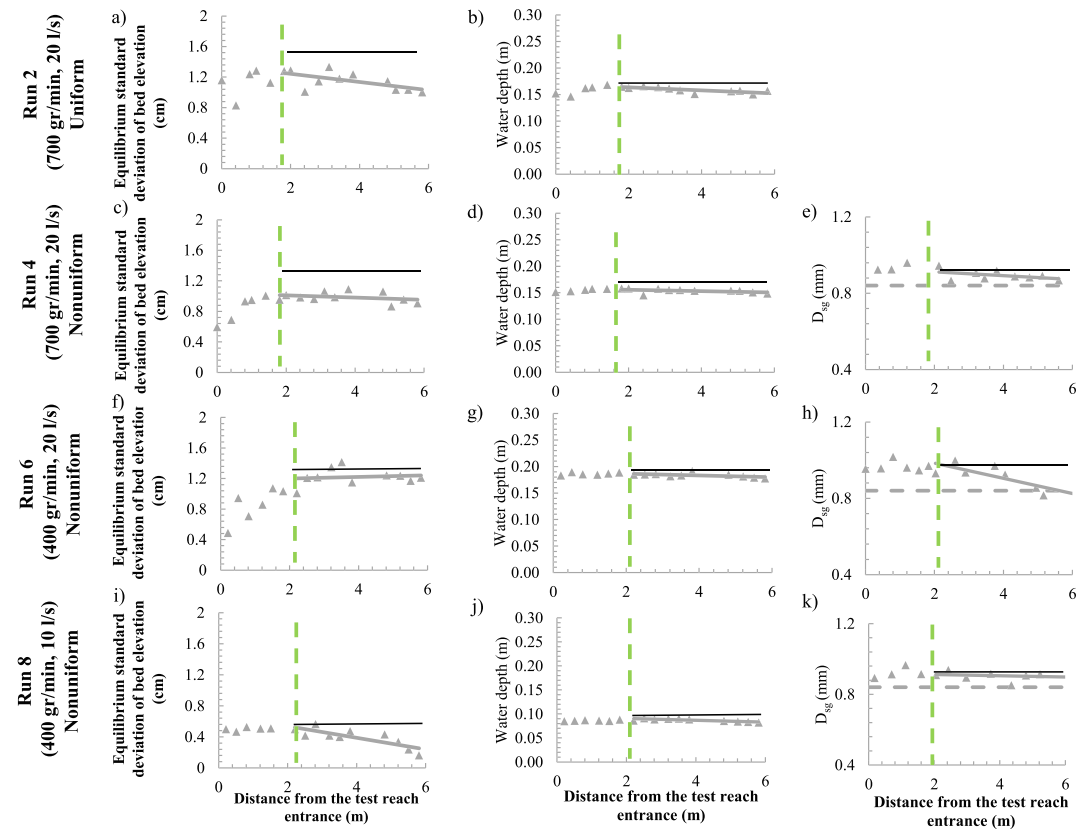


Figure 7. Spatial changes in equilibrium standard deviation of the bed elevation, σ_η , water depth, H , and geometric mean diameter of the surface sediment, D_{sg} , in the runs with exposed bedrock (Runs 2, 4, 6, and 8). Symbols represent the experimental points. The black lines are the fully alluvial values downstream of the bedform development region. The dashed green lines indicate the location of the stable alluvial-bedrock transition. The gray lines are regression lines on the exposed bedrock data points.

Run 1 (Figure 5a), which was performed with uniform sand and the same flow and feed rates of Run 3, the bedform development region was ~ 4.5 m long. This notwithstanding, a similarly large difference in σ_η between Runs 1 and 3 was not observed. The equilibrium σ_η was respectively equal to 1.5 cm and 1.3 cm. Whether or not the presence of relatively coarse sediment in the nonuniform sediment or the difference in D_g between the uniform and the nonuniform material played a significant role on the length of the bedform development region remains an open question.

The equilibrium flow depth is presented in Figure 5 (b, d, g, and j). In all the experiments, the water depth increased in the streamwise direction in the bedform development region, and it became constant in space where the bedforms were fully developed. The regression slopes for the water depth in bedform development region are 0.0004, 0.0047, 0.0055, and 0.0033 for Runs 1, 3, 5, and 7, respectively, showing a streamwise increase of flow depth. In the bedform development region, σ_η , and thus the flow resistances, increased in the flow direction, and this corresponded to increasing flow depths. The slopes of the regression lines of Figure 5 (b, d, g, and j) are smaller than 0.001 cm/m showing that water depth can be reasonably considered uniform downstream of the bedform development region.

The equilibrium D_{sg} is presented in Figure 5 (e, h, and k) where the slopes of the regression lines are smaller than 0.01 mm/m. The equilibrium bed surface was generally coarser than the sediment supply to regulate the mobility of the fine and coarse sediment (Parker & Klingeman, 1982; Paola et al., 1992). In the fully alluvial reach downstream of the bedform development region, the equilibrium D_{sg} did not change in space.

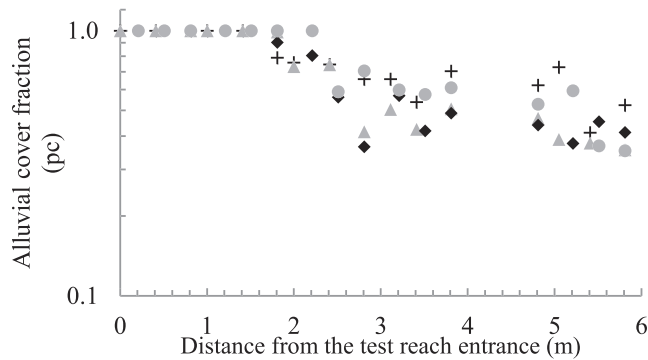


Figure 8. Streamwise changes of the equilibrium alluvial cover fraction, p_c . Black pluses, gray triangles, black diamonds, and gray circles, respectively, represent p_c for Run 2 (700 g/min, 20 l/s, uniform), Run 4 (700 g/min, 20 l/s, nonuniform), Run 6 (400 g/min, 20 l/s, nonuniform), and Run 8 (400 g/min, 10 l/s, nonuniform).

4.2. Equilibrium With Exposed Bedrock

The results of the experiments with an equilibrium bedrock reach are summarized in Figure 7, which is analogous to Figure 5. Equilibrium data are presented in terms of streamwise changes in standard deviation of bed elevation σ_η (a, c, f, and i), water depth H (b, d, g, and j), and geometric mean diameter of the bed surface sediment D_{sg} (e, h, and k).

Due to the limited length of the test reach, water level at the downstream boundary in the mixed bedrock-alluvial runs was chosen so that the length of the alluvial reach was of comparable length with that of the bedform development region observed in the fully alluvial runs with nonuniform bed material, i.e., ~ 2 m (Figure 5).

Figure 7 (a, c, f, and i) shows the streamwise variation of σ_η at equilibrium. In Run 2 (Figure 7a), σ_η grew in the alluvial reach with values that were comparable with those measured in the paired fully alluvial equilibrium run (Run 1). Due to the interaction with the model bedrock, σ_η decreased in the flow direction in the bedrock reach (0.051 m/m). A similar stream-

wise decrease of σ_η (0.07 m/m) was observed in Run 8 (flow rate 10 l/s and feed rate 400 g/min, Figure 7i). In Run 4, which was performed with the same flow rate and feed rate of Run 2 but with nonuniform sand, σ_η was smaller than in the paired fully alluvial run and gently (0.022 m/m) decreased in the streamwise direction in the bedrock reach. Finally, in Run 6 with flow rate equal to 20 l/s and feed rate equal to 400 g/min, σ_η did not seem to significantly change from the alluvial equilibrium value and remained uniform in the bedrock reach (0.009 m/m) (Figure 7f).

Panels b, d, g, and j of Figure 7 show the changes in water depth in the bedrock reaches compared to the fully alluvial cases. In the runs with feed rate equal to 700 g/min, i.e., Run 2 and Run 4 (Figure 7b and 7d), a change in water depth as compared to the paired fully alluvial runs is clearly visible. In particular, in the run with uniform bed material (Run 2), the water depth at the end of the alluvial reach was similar to the water depth in the corresponding fully alluvial run (Run 1), while downstream on the alluvial-bedrock transition, the interaction with the model bedrock resulted in a water depth that decreased in the flow direction at a rate of 0.0028 m/m (Figure 7b). In the run with nonuniform bed material and a feed rate equal to 700 g/min (Run 4), the water depth at the end of the alluvial reach was smaller than in the paired alluvial run (Run 3), and then it gently decreased (0.0019 m/m) in the streamwise direction in the bedrock reach (Figure 7d). In the runs with a feed rate equal to 400 g/min, i.e., Runs 6 and 8 (Figure 7g and 7j), the water depths decreased very gently in the flow direction in the bedrock reach (0.0018 m/m in Run 6 and 0.0023 m/m in Run 8).

The response of the flow to the presence of the model bedrock showed that the distance between the water level at the downstream boundary and the bedrock, ξ_d , plays a prime control on the equilibrium flow characteristics in the bedrock reach. In Runs 2 and 4, ξ_d was approximately 90% of the alluvial equilibrium depth H_o observed in the paired runs, and this forced the equilibrium flow depth to clearly decrease in the streamwise direction compared to the fully alluvial case. In Runs 6 and 8, ξ_d was respectively equal to $0.96H_o$ and H_o , not enough to cause a visible flow acceleration in our relatively short test reach.

Panels e, h, and k show the spatial changes of D_{sg} in the streamwise direction. In Runs 4 and 8, there was no significant change of D_{sg} compared to the alluvial equilibrium runs, but a very mild pattern of downstream fining was observed in Run 4 (0.01 mm/m) and in Run 8 (0.0034 mm/m). On the contrary, in Run 6 (flow rate 20 l/s and feed rate 400 g/min), a clear pattern of downstream fining was observed in the bedrock reach (0.051 mm/m) (Figure 7h). These results suggest that in the runs in which σ_η decreased in streamwise direction, i.e., Runs 4 and 8, there was a small streamwise change of the geometric mean diameter of the surface material as compared to the paired alluvial runs. On the other hand, in the run with σ_η close to the alluvial equilibrium value, a stable pattern of downstream fining formed on the bed surface.

The spatial change in alluvial cover at equilibrium is presented in Figure 8. When the alluvial cover was equal to 1, the reach was fully alluvial, while exposed bedrock was observed when the alluvial cover is smaller than 1. Significant changes in alluvial cover fraction between the experimental runs were not observed

suggesting that the streamwise distance between the alluvial-bedrock transition and the end of the test reach might have had a significant control on the fraction of exposed bedrock.

4.3. Summary of the Experimental Results

In our experiments the interaction of the bedrock surface with the flow hydrodynamics and the sediment transport processes varied depending on ξ_d . When ξ_d was close to the alluvial equilibrium flow depth H_o (Runs 6 and 8), changes in flow depth and flow velocity from the alluvial equilibrium values were negligibly small in the bedrock reach. On the contrary, when ξ_d was significantly smaller than the alluvial equilibrium depth, a shallower flow depth than in the paired alluvial runs and spatial flow acceleration was observed in the bedrock reaches (Figures 7b and 7d).

The observed spatial changes in water depth partially confirm the numerical predictions of the Viparelli et al. (2015) formulation, i.e., at equilibrium in a low slope bedrock reach downstream of an alluvial-bedrock transition, the flow is characterized by a reduction of the flow depth in the streamwise direction. The experimental results however showed that the problem is more complex than in the Viparelli et al. (2015) formulation due to the changes in bedform geometry and grain size distribution of the alluvial bed surface, which can occur even with very small changes in flow depth and velocity.

The interaction between flow hydrodynamics, bedload transport, and model bedrock resulted in two different responses, a streamwise decrease in σ_η in Runs 2, 4, and 8 and the formation of a stable pattern of downstream fining in Runs 4 and 6. It is important to note here that in Run 4, both the streamwise decrease in σ_η and the pattern of downstream fining were milder than those observed in the other runs, which were either characterized by a change in σ_η or by downstream fining of the bed surface sediment.

In a sediment feed flume, the equilibrium bedload transport rate must be equal to the sediment feed rate (equation 1). Due to the presence of exposed bedrock, the bed material transport capacity in the bedrock reaches should be higher than the bed material transport capacity in the alluvial reaches (Sklar & Dietrich, 2004; Zhang et al., 2015). Recalling that the bed material transport capacity is an increasing function of the bed shear stress associated with skin friction (Fernandez Luque & Van Beek, 1976; Parker, 2008), we hypothesize that in mixed bedrock-alluvial runs, the observed changes in bedform geometry and grain size distribution of the bed surface sediment may result in higher bedload transport capacities compared to the paired fully alluvial runs.

Noting that (1) ξ_d in Runs 6 and 8 was very close to the alluvial equilibrium values, (2) Run 6 was characterized by uniform σ_η and a stable pattern of downstream fining, and (3) σ_η decreased in the streamwise direction without spatial changes of D_{sg} in Run 8, we hypothesize that ξ_d cannot be the only control on bedform regime and the sediment sorting patterns in the bedrock reach.

5. Discussion

To test the hypotheses presented above, the discussion section is organized in four parts. In part 1 we compute the spatial changes in flow resistances and bed shear stresses in the bedrock reach to determine if the observed changes in bedform geometry and grain size distribution of the bed surface sediment correspond to higher bedload transport capacities than at alluvial equilibrium. We then discuss how flow acceleration downstream of a stable alluvial-bedrock transition results in the formation of a pattern of downstream fining of the bed surface sediment. The bed shear stresses computed in part 1 are then used to determine if size-specific bedload transport relations for fully alluvial systems can be reasonably applied to model bedload transport of nonuniform sediment in bedrock reaches. Finally, in part 4 we use one of the Vanoni (1975) bedform diagrams to compare the bedform characteristics observed in the bedrock reaches with those observed in the paired fully alluvial cases.

5.1. Spatial Changes in Flow Resistances and in Bed Shear Stress in the Bedrock Reaches

The experiments presented in sections 3 and 4 indicate that in the bedrock reach, either the grain size distribution of the bed surface sediment, or the bedform geometry, or both were different from those measured at equilibrium in the paired alluvial runs. We thus expect that the flow resistances and consequently the bed shear stresses in the bedrock runs are different from their alluvial equilibrium values.

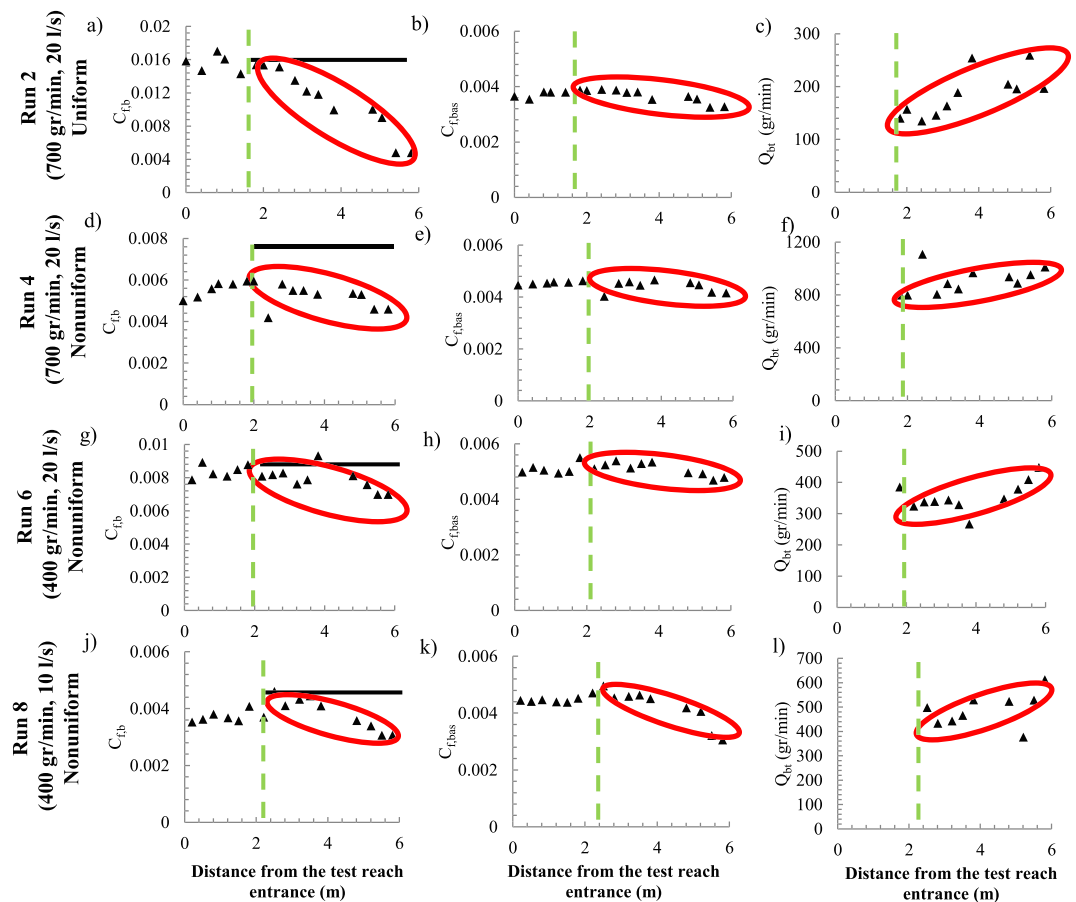


Figure 9. Streamwise changes of the equilibrium total, sidewall corrected friction coefficient $C_{f,b}$ (a, d, g, and j), friction coefficient associated with skin friction for the alluvial patches, $C_{f,bas}$ (b, e, h, and k), and sediment transport capacity over the exposed bedrock reach, Q_{bT} (c, f, i, and l). The green line denotes the location of alluvial-bedrock transition. The black lines represent fully alluvial values downstream of the alluvial-bedrock transition, and the red ovals show the values in exposed bedrock runs downstream of the alluvial-bedrock transition.

The calculation of the bed shear stress and of the flow resistance was not straightforward. To account for the different roughness between the smooth sidewalls and the rough bed, the procedure suggested by Vanoni and Brooks (1957) was followed, as summarized in text S1 of the Supporting Information. Further, to compute the resistance in the mixed bedrock-alluvial areas, the procedure proposed by Johnson (2014) was used. The alluvial resistance was then partitioned between skin friction and form drag with an Einstein decomposition of the sidewall corrected alluvial values, as illustrated in Supporting Information text S2 (Parker, 2004).

The results of this analysis are presented in Figure 9 in terms of total, sidewall corrected friction coefficients $C_{f,b}$ (panels a, d, g, and j), friction coefficients associated with skin friction on the alluvial patches $C_{f,bas}$ (panels b, e, h, and k), and sediment transport capacity in bedrock reaches Q_{bT} (panels c, f, i, and l).

a Spatial Changes in Total (Sidewall Corrected) Bed Friction Coefficient

Panels a, d, g, and j of Figure 9 show that the total, sidewall corrected friction coefficient, $C_{f,b}$, in the runs with exposed bedrock decreases in the streamwise direction. There are two reasons associated with this: (1) the decrease in roughness height caused by the downstream fining of the bed surface material (Runs 4 and 6) and by the streamwise decrease in σ_η (Runs 2, 4, and 8) and (2) an increase of the areal fraction of the exposed bedrock, which was characterized by a smaller roughness height than the alluvial patches. The characteristic roughness height of the model bedrock was ~ 0.1 mm, and the grain roughness height of the alluvial patches was assumed to be a function of D_{s90} , i.e., the diameter such that 90% of the bed

surface sediment was finer. Therefore, as the fraction of exposed bedrock increased, the composite roughness became smaller, and consequently the friction coefficient decreased in streamwise direction for all bedrock runs.

b Spatial Changes in Flow Resistances Associated With Skin Friction

In the Johnson (2014) formulation to compute flow resistances in mixed bedrock-alluvial reaches, the side-wall corrected bed friction coefficient $C_{f,b}$ (see Supporting Information for the calculation procedure) was defined as a weighted average between the friction coefficient for the alluvial areas and for the exposed bedrock areas.

$$C_{f,b} = p_c C_{f,ba} + (1-p_c) C_{f,bb}, \quad (2)$$

where $C_{f,ba}$ is the friction coefficient associated with the alluvium and $C_{f,bb}$ is the friction coefficient associated with the bedrock. To partition the flow resistances between the alluvial patches and the exposed bedrock, we applied a procedure similar to the procedure used to partition the flow resistances in alluvial rivers between skin friction and form drag (Parker, 2004 and references therein). We considered an ideal flow over a rough bed with the same roughness of the bedrock surface. The energy slope and mean flow velocity of this ideal flow were assumed to be equal to the energy slope and the mean flow velocity of the flow in the presence of alluvial patches, i.e., of the experimental runs. The friction coefficient for the exposed bedrock was thus computed as:

$$C_{f,bb}^{-1/2} = \alpha_r \left(\frac{r_{b,b}}{k_{sb}} \right)^{1/6}, \quad (3)$$

with k_{sb} denoting the roughness height of the bedrock (0.1 mm) and $r_{b,b}$ the hydraulic radius of the ideal flow over the bedrock surface. α_r is a constant equal to 8.1 (Parker, 1991). Using a Manning-Strickler formulation, $r_{b,b}$ was computed as:

$$r_{b,b} = \left(\frac{k_{sb}^{1/6} U}{\alpha_r \sqrt{g S_f}} \right)^{3/2}, \quad (4)$$

with U being the cross-sectionally averaged flow velocity and S_f the friction slope. Using equations (2)–(4), we computed the friction coefficient of the alluvial areas, which accounts for flow resistances associated with both skin friction and form drag $C_{f,ba}$. We then partitioned the alluvial flow resistances between skin friction and form drag, as illustrated in the Supplementary Information. The friction coefficient associated with skin friction, $C_{f,bas}$, was finally used to compute the sediment transport capacities. Panels b, c, h, and k of Figure 9 show the spatial variation of the friction coefficient associated with skin friction for the alluvial areas, which in the bedrock reaches is gently decreasing in streamwise direction.

c Spatial Changes in Sediment Transport Capacity in the Bedrock Reach

The sediment transport capacity Q_{bT} was computed with the relation of Ashida and Michiue (Parker, 2008) for uniform material equal to the geometric mean size D of the sediment feed as:

$$Q_{bT} = B \sqrt{RgDD} \cdot 17 (\tau_{bas}^* - 0.05) \left(\sqrt{\tau_{bas}^*} - \sqrt{0.05} \right), \quad (5)$$

where B is the flume width, R denotes the submerged specific gravity of the sediment equal to 1.65 in the present calculations, g is the acceleration of gravity, and τ_{bas}^* represents the Shields stress on the alluvial patches associated with skin friction, equal to $C_{f,bas} U^2 / RgD$.

The streamwise variability of Q_{bT} in the runs with exposed bedrock is presented in Figure 9 (c, f, i, and l). In the bedrock reaches, Q_{bT} clearly increases in the streamwise direction, in response to the reduction of alluvial cover of Figure 8.

The results of Figures 7–9 show that the response of the flow and of the bedload transport to the presence of an un-erodible surface is more complex than that presented in Zhang et al. (2015) and Viparelli et al. (2015).

Notwithstanding the streamwise reduction of the flow resistances (Figures 9a, 9b, 9d, 9e, 9g, 9h, 9j, and 9k), downstream of the stable alluvial-bedrock transitions, the bed material transport capacity tends to increase in the direction of the flow (Figure 9c, 9f, 9i, and 9l).

5.2. Stable Pattern of Downstream Fining Downstream of a Stable Alluvial-Bedrock Transition

The formation of a stable pattern of downstream fining downstream of the stable bedrock-alluvial transition can be considered a consequence of the streamwise increase in bed material transport capacity discussed in the previous section. Parker and Klingeman (1982) noticed the formation of a coarse pavement at equilibrium in a fully alluvial system transporting nonuniform bed material. This pavement is a thin layer on the topmost part of the deposit that regulates the different mobility of coarse and fine grains. In particular, the overrepresentation of coarse grains compensates for their relatively small mobility so that at equilibrium the bedload transport rate is everywhere equal to the bedload transport capacity and the feed rate (Parker & Klingeman, 1982). The formation of a coarse pavement in our fully alluvial experiments is shown in Figure 5 (panels c, h, and k).

The streamwise increase in bed material transport presented in Figure 9 is the result of the streamwise increase of the bed shear stress associated with skin friction, τ_{bas} , (see equation (5)) in the bedrock reaches. Thus, as τ_{bas} increases in the streamwise direction, the mobility difference between coarse and fine grains becomes less pronounced, and, as a consequence, the grain size distribution of the pavement tends to become similar to the grain size distribution of the load (Viparelli et al., 2011). In other words, as the bed shear stress associated with skin friction increases downstream of a stable alluvial-bedrock transition, the bed surface tends to become unarmored with the consequent formation of a stable pattern of downstream fining, as reported by Nittrouer (2013) for the lower Mississippi River.

5.3. Comparison Between the Experimental Results and the Ashida and Michiue Bedload Transport Relation

To determine if surface-based bedload relations for fully alluvial systems can be reasonably used to predict grain size-specific bedload transport rates in bedrock reaches, we compared our experimental data with bedload transport rates predicted using the surface-based version of the *Ashida and Michiue* relation (Parker, 2008), which is appropriate to model bedload transport in alluvial reaches transporting sand and pea gravel.

The surface-based form of the *Ashida and Michiue* bed load relation takes the form:

$$q_{bsi}^* = 17(\tau_{bsi}^* - \tau_{refi}^*) \left(\sqrt{\tau_{bsi}^*} - \sqrt{\tau_{refi}^*} \right), \quad (6)$$

where q_{bsi}^* represents dimensionless transport rate per unit width of sediment with characteristic grain size D_i , τ_{bsi}^* is the size-specific Shields number associated with skin friction defined as the ratio between the alluvial bed shear stress associated with skin friction and $\rho R g D_i$, with ρ the water density, R the submerged specific gravity of the sediment and g the acceleration of gravity, while τ_{refi}^* denotes reference Shields number for the sediment particles with characteristic grain size D_i , computed with the following hiding/exposure function (Parker, 2008).

$$\frac{\tau_{refi}^*}{\tau_{scg}^*} = \begin{cases} 0.843 \left(\frac{D_i}{D_{sg}} \right)^{-1} & \text{for } \frac{D_i}{D_{sg}} \leq 0.4 \\ \left[\frac{\log(19)}{\log\left(19 \frac{D_i}{D_{sg}}\right)} \right]^2 & \text{for } \frac{D_i}{D_{sg}} < 0.4 \end{cases}, \quad (7)$$

in which τ_{scg}^* is a reference value equal to 0.05.

The grain size-specific volumetric bedload transport rate per unit channel width is computed using the definition of dimensionless transport rate per unit channel width as:

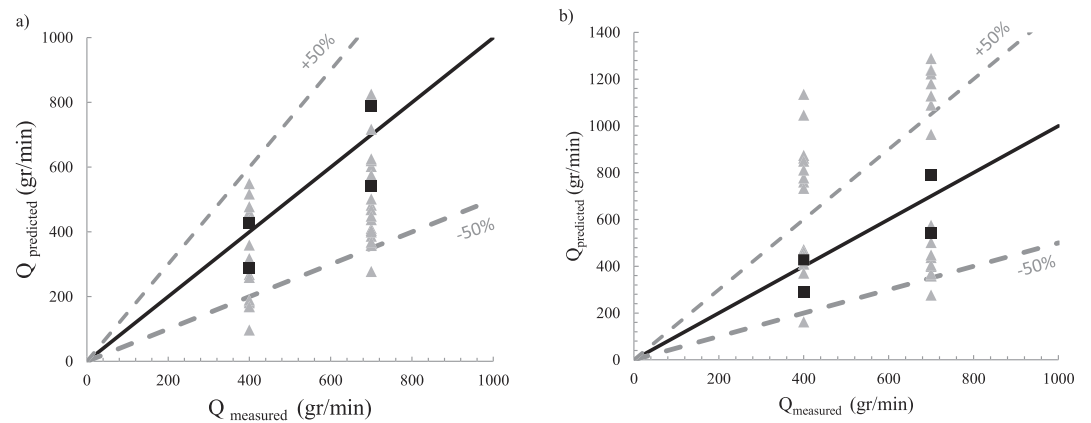


Figure 10. Comparison between the measured (horizontal axis) and predicted (vertical axis) bedload transport rates per unit width. Predictions are done with the Ashida and Michiue bedload relation multiplied by the measured alluvial cover fraction. The gray triangles are the points pertaining to experimental runs with exposed bedrock, and the black squares represent fully alluvial runs. The black line corresponds to perfect equality, and the dashed lines indicate $\pm 50\%$ difference between measured and predicted values.

$$q_{bi} = \sqrt{RgD_i} p_c F_i q_{bsi}^* \quad (8)$$

where F_i denotes the volume fraction content of sediment with characteristic grain size D_i in the bed surface. The only difference of this relation with relations for fully alluvial systems is the presence of p_c in the right-hand side, which accounts for the reduced availability of alluvial sediment associated with the presence of exposed bedrock. The total sediment transport rate per unit width is then computed as the sum of q_{bi} over all the grain size fractions.

$$q_{bT} = \sum_{i=1}^n q_{bi} \quad (9)$$

where n denotes the number of characteristic grain sizes.

The comparison between experimental and computed bedload transport rates is presented in Figure 10, where the black squares represent the alluvial equilibrium experiments and the gray triangles refer to equilibrium conditions in the mixed bedrock-alluvial reaches. The equilibrium bedload transport rate in the experiments, which was equal to the sediment feed rate, is on the horizontal axis of Figure 10, while the results of the calculations performed with equations (6)–(9) are reported on the vertical axis. The continuous line represents perfect equality, and the dashed lines identify the 50% error from the measured value. In Figure 10a, the alluvial cover fraction (p_c) is accounted for in the calculations, while the bedload calculations of Figure 10b were performed without considering the cover fraction parameter. The results clearly show that the cover fraction (i.e., the availability of alluvial sediment) has to be accounted for in bedload transport calculations.

When the alluvial cover fraction is accounted for, the difference between experimental and predicted values of bedload transport rates is in the majority of the cases within the $\pm 50\%$ error, which is comparable with the error of other bedload transport rate predictors for nonuniform sediment (Parker, 1990; Wilcock & Crowe, 2003). Thus, the surface-based version of the *Ashida and Michiue* bedload transport relation reasonably reproduces the bedload transport rates measured during the experiments. It is expected that other bedload transport models derived for alluvial systems can be used to predict the total, i.e., summed over all the grain sizes, bedload transport rates in bedrock rivers if the bedload transport capacity is multiplied by the alluvial cover fraction (Sklar & Dietrich, 2004).

To determine if the *Ashida and Michiue* surface-based relation was able to adequately model the grain size-specific sediment fluxes, we used equations (6)–(9) to predict the equilibrium grain size distribution of the surface material in the bedrock reaches, as outlined by Parker and Sutherland (1990) for fully alluvial

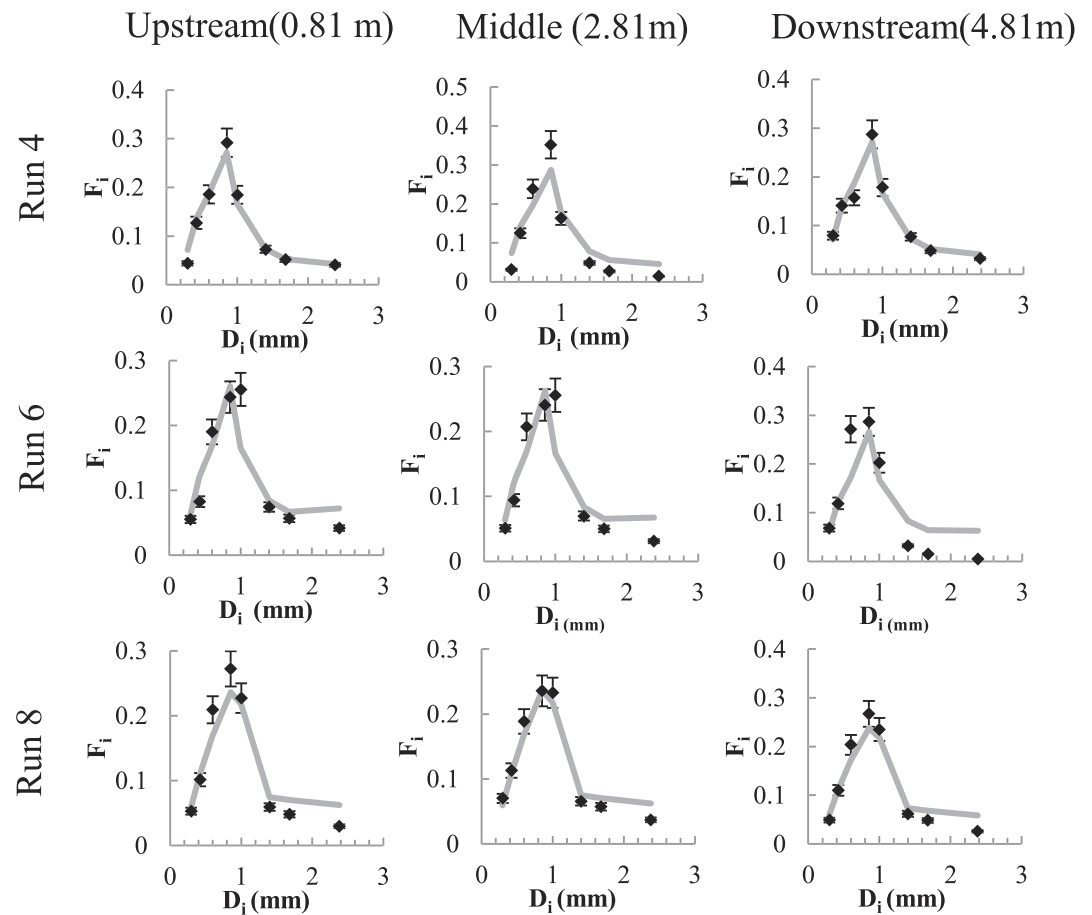


Figure 11. Comparison between measured and predicted grain size distributions of the bed surface sediment. The black dots are the experimental data, and the continuous gray lines are the sediment size distributions predicted with the Ashida and Michiue bedload transport relation. The error bars indicate a 10% error.

systems. The only difference between the procedure used herein and that presented by *Parker and Sutherland* (1990) is that our grain size-specific bedload transport capacities are multiplied by the alluvial cover fraction p_c .

The comparison between predicted and measured grain size distributions of the bed surface sediment is presented in Figure 11 for three different locations, i.e., ~0.81 m, ~2.81 m, and ~4.81 m from the test reach entrance. The comparison between model predictions and experimental data reveals a reasonably good agreement between measured and predicted equilibrium grain size distributions of the bed surface sediment. The prediction errors of the grain size distributions of the bed surface sediment are comparable with those of surface-based models in alluvial systems (e.g., *Parker & Sutherland*, 1990). These results further confirm that grain size-specific bedload transport models derived for fully alluvial systems can be reasonably used to model grain size-specific bedload transport in bedrock reaches if the bed material transport capacities are multiplied by the alluvial cover.

5.4. Changes in Bed Configuration

To test the hypothesis that the observed changes in σ_η and/or grain size distribution of the bed surface sediment are not solely controlled by the distance between the water surface base level and the bedrock surface, ξ_d , we used the *Vanoni* (1975) diagram for sediment sizes of 0.93 mm, 1.2 mm, and 1.35 mm. The vertical axis of the *Vanoni* (1975) diagram is Froude number, defined as $U/(gH)^{0.5}$ with U denoting the mean flow velocity, g acceleration of gravity, and H the flow depth. The horizontal axis is the ratio between water depth and grain size of the bed material, set equal to D_{sg} in the runs with nonuniform sediment.

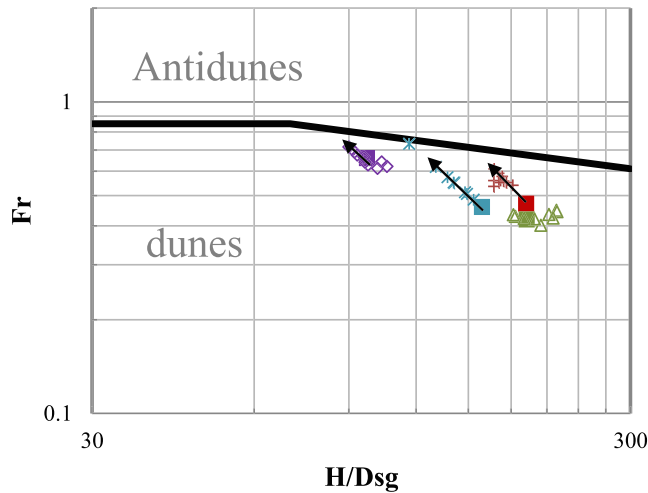


Figure 12. Vanoni [1975] diagram for bedform regime (grain size diameters of 0.93 mm, 1.20 mm, and 1.35 mm). Blue stars are the points in Run 2, red pluses are the points in Run 4, green triangles are the points in Run 6, and the purple diamonds are the Run 8. Fully alluvial runs, i.e., Runs 1, 3, 5, and 7 are, respectively, shown with blue, red, green, and purple squares.

The Vanoni (1975) diagram is presented in Figure 12 where the black lines represent the transition between dunes and antidunes and the symbols are our experimental points. In Runs 2, 4, and 8, which were characterized by smaller values of σ_η in the bedrock reaches than in the paired fully alluvial runs, the bedform diagram of Figure 12 suggests that the observed change in bedform shape was associated with a change in bed configuration from the dune regime toward upper regime plane bed at the dune-antidune transition. In Run 6 significant changes in σ_η from the alluvial equilibrium case were not observed, and this corresponded to no significant change in the bedform regime at equilibrium in the bedrock reach (green triangles in Figure 12).

Recalling that ξ_d in Runs 2, 4, 6, and 8 was respectively equal to $0.9H_o$, $0.9H_o$, H_o , and $0.97H_o$, respectively, Figure 12 suggests that when ξ_d is significantly smaller than the alluvial equilibrium flow depth (Runs 2, blue asterisks, and Run 4, red pluses), the interaction between the bedrock surface and the bedforms results in bedform configurations that are closer to the dune-antidune transition and with smaller bedform heights than in the fully alluvial case. When ξ_d is close to the equilibrium flow depth and the bedform regime is close to the dune-antidune transition (Run 8, purple diamonds), the interaction between the bedrock surface and the bedforms results in bedform characteristics that are closer to antidunes than in the

alluvial case. When ξ_d is close to the alluvial equilibrium flow depth and the bedforms are well in the dune regime (Run 6, green triangles), no changes in σ_η and bedform regime should be expected. Finally, when the alluvial equilibrium bed configuration is far from the dune-antidune transition (Runs 3 and 5), the formation of a stable pattern of downstream fining in the bedrock reach can be expected (Runs 4 and 6).

It is important to note here that the experimental conditions were close to the dune-antidune transition in the absence of suspended bed material load, thus should be representative of relatively small and steep rivers transporting medium to coarse sand (Wright & Parker, 2004). This notwithstanding, the experimental results provide general information on the interactions between lower regime bedforms and a bedrock surface, i.e., bedform characteristics in a low slope bedrock reach may be significantly different than in a fully alluvial reach subject to the same flow regime and sediment supply. New experiments and field data are necessary to confirm the experimental observations and fully understand the complex interaction between bedload transport of nonuniform material and bedform characteristics in low slope, sand bed bedrock reaches.

6. Conclusions

We performed laboratory experiments on the equilibrium of low slope bedrock channels transporting nonuniform sand. The experiments provided novel and quantitative insight on the flow characteristics, bedform geometry, longitudinal sorting patterns, and flow resistances in bedrock reaches, notwithstanding the limited length of the test reach.

In equilibrium bedrock reaches downstream of an alluvial-bedrock transition, i.e., when the slope of the bedrock surface is milder than the equilibrium slope of an alluvial system subject to the same flow regime and sediment supply, the interaction between the bedrock, the flow characteristics, and the sediment transport may result in:

- I Flow acceleration (Figure 7b, 7d, 7g, and 7j) in the streamwise direction. This spatial flow acceleration is associated with a decreasing alluvial cover in the direction of the flow.
- II Changes in bedform geometry compared to the alluvial equilibrium case. In bedrock reaches, σ_η which is the spatio-temporal sequence of bedform geometry tends to be smaller than in the fully alluvial case and, due to the flow acceleration, it may decrease in the flow direction (Figure 7 a, c, f, i).
- III Formation of a stable pattern of downstream fining of the bed surface sediment in response to the flow acceleration in the bedrock reach (Figure 7e, 7h, and 7k). This can be explained noting that as bedload transport capacity increases in the streamwise direction, the bed surface tends to become unarmored (Parker and Klinegman, 1982);

The observed streamwise decrease in σ_η and/or bed surface grain size observed in the experiments results in a streamwise decrease in the flow resistances. This streamwise decrease of flow resistances is associated with an increase of the bed material transport capacity in the bedrock reach, which balances the streamwise reduction in alluvial cover fraction.

Surface-based formulations of grain size-specific bedload transport models are able to reasonably reproduce the grain size-specific bedload transport rates in bedrock reaches, if the alluvial cover is used to balance the higher bedload transport capacities associated with the spatial flow acceleration.

The response of the bedforms and of the bed surface sediment to the presence of a nonerodible surface seems to depend on the distance between the water surface base level and the bedrock surface, ξ_d , and to the bedform regime (Figure 12). If ξ_d is significantly smaller than the alluvial equilibrium flow depth or the alluvial equilibrium bedforms are close to the dune-antidune transition, a streamwise reduction in σ_η can be expected in the bedrock reach. If the alluvial equilibrium bedforms are well in the dune regime and ξ_d is close to the alluvial equilibrium flow depth, the formation of a stable pattern of downstream fining of the bed surface sediment in the bedrock reach can be expected.

Notation

C_f	Friction coefficient
$C_{f,ba}$	Friction coefficient associated with alluvium
$C_{f,bas}$	Friction coefficient of alluvial cover associated with skin friction
$C_{f,bb}$	Friction coefficient associated with bedrock
C_{fb}	Side wall corrected friction coefficient
D_g	Geometric mean diameter of the sediment supply
D_i	Grain size diameter
D_{sg}	Geometric mean diameter of the surface material
F_i	Volume fraction content of sediment for generic grain sizes
Fr	Froude number
g	Acceleration of gravity
H	Water depth
H_o	Equilibrium water depth
K_{sb}	Roughness height of the bedrock
L_{ac}	Minimum thickness of alluvial cover
P_c	Alluvial cover fraction
q_{bsi}^*	Nondimensional bedload transport rate per unit width for a generic grain size
q_b	Bedload transport rate per unit channel width
q_{bi}	Bedload transport rate per unit width for generic grain sizes
q_{bm}	Volumetric bed material load per unit channel width
q_{bT}	Total bedload transport rate per unit width
q_c	Sediment transport capacity
R	Submerged specific gravity
$R_{h,b}$	Hydraulic radius of ideal flow over bedrock surface
S_b	Bedrock slope
S_f	Friction slope
S_o	Equilibrium bed slope
U	Averaged flow velocity
η_a	Average elevation of alluvial deposit
η_b	Bedrock elevation
η_{bd}	Bedrock elevation at the downstream
λ_p	Bed material porosity
ξ_d	Water level at the downstream boundary
ρ	Water density
σ_g	Standard deviation of the sediment supply
σ_n	Standard deviation of the bed elevation

τ^*	Nondimensional shear stress
τ_{bas}^*	Nondimensional shear stress of alluvial cover associated with skin friction
τ_{bsi}^*	Nondimensional shear stress associated with skin friction for a generic grain size
τ_{refi}^*	Reference shields number for generic grain sizes
τ_{scg}^*	Grain size nonspecific reference value for shields number
τ_b	Bed shear stress
τ_{bas}	Shear stress of alluvial cover associated with skin friction

Notation for Supporting Information

A_b	Area of the bed region
A_{cs}	Cross-sectional area
A_w	Area of the wall region
$C_{f,b}$	Friction coefficient of bed region
$C_{f,cs}$	Friction coefficient of cross section
$C_{f,w}$	Friction coefficient of wall region
f_w	Friction factor of wall region
P_b	wetted perimeter of bed region
P_{cs}	wetted perimeter of cross section
P_w	Wetted perimeter of wall region
r_b	Hydraulic radius of bed region
r_{cs}	Hydraulic radius of cross section
Re_b	Reynolds number of bed region
Re_{cs}	Reynolds number of cross section
Re_w	Reynolds number of wall region
r_w	Hydraulic radius of wall region

Acknowledgments

The authors thank the University of South Carolina geotechnical engineering group for providing access to the equipment to perform sieve analyses, Jeff Nittrouer, Michele Bolla Pittaluga, and two anonymous reviewers for comments and suggestions on earlier versions of the manuscript. This research was supported by the United States National Science Foundation through award EAR 1250641 and by the University of South Carolina. The dataset has been made publicly available through the assistance of the Sediment Experimentalist Network (SEN) at the SEAD website (<http://doi.org/10.5967/M0VH5KTM>).

References

- Anderson, A. G., Parker, G., & Wood, A. (1975). The flow and stability characteristics of alluvial river channels.
- Blom, A., Parker, G., Ribberink, J. S., & De Vriend, H. J. (2006). Vertical sorting and the morphodynamics of bed-form-dominated rivers: An equilibrium sorting model. *Journal of Geophysical Research*, *111*, F01006. <https://doi.org/10.1029/2004JF000175>
- Blom, A., Viparelli, E., & Chavarrias, V. (2016). The graded alluvial river: Profile concavity and downstream fining. *Geophysical Research Letters*, *43*, 6285–6293. <https://doi.org/10.1002/2016GL068898>
- Carling, P. A., Golz, E., Orr, H. G., & Radecki-Pawlik, A. (2000). The morphodynamics of fluvial sand dunes in the River Rhine, near Mainz, Germany. I. *Sedimentology and morphology*. *Sedimentology*, *47*(1), 227–252. <https://doi.org/10.1046/j.1365-3091.2000.00290.x>
- Carling, P. A., Williams, J. J., Golz, E., & Kelsey, A. D. (2000). The morphodynamics of fluvial sand dunes in the River Rhine, near Mainz, Germany. II. Hydrodynamics and sediment transport. *Sedimentology*, *47*(1), 253. <https://doi.org/10.1046/j.1365-3091.2000.00291.x>
- Chatanantavet, P., & Parker, G. (2008). Experimental study of bedrock channel alluviation under varied sediment supply and hydraulic conditions. *Water Resources Research*, *44*, W12446. <https://doi.org/10.1029/2007WR006581>
- Chatanantavet, P., & Parker, G. (2009). Physically based modeling of bedrock incision by abrasion, plucking, and macroabrasion. *Journal of Geophysical Research*, *114*, F04018. <https://doi.org/10.1029/2008JF001044>
- Chatanantavet, P., Whipple, K. X., Adams, M. A., & Lamb, M. P. (2013). Experimental study on coarse grain saltation dynamics in bedrock channels. *Journal of Geophysical Research: Earth Surface*, *118*, 1161–1176. <https://doi.org/10.1002/jgrf.20053>
- Chen, Z., & Stanley, D. J. (1993). Alluvial stiff muds (late Pleistocene) underlying the lower Nile delta plain, Egypt: Petrology, stratigraphy and origin. *Journal of Coastal Research*, 539–576.
- Engelund, F., & Hansen, E. (1967). A monograph on sediment transport in alluvial streams. Technical University of Denmark Ostervoldgade 10, Copenhagen K.
- Fernandez Luque, R., & Van Beek, R. (1976). Erosion and transport of bed-load sediment. *Journal of hydraulic research*, *14*(2), 127–144. <https://doi.org/10.1080/00221687609499677>
- Finnegan, N. J., Sklar, L. S., & Fuller, T. K. (2007). Interplay of sediment supply, river incision, and channel morphology revealed by the transient evolution of an experimental bedrock channel. *Journal of Geophysical Research*, *112*, F03S11. <https://doi.org/10.1029/2006JF000569>
- Garcia, M. H. (2008). Sediment transport and morphodynamics. In *sedimentation engineering: Processes, measurements, modeling, and practice* (pp. 21–163). <https://doi.org/10.1061/9780784408148.ch02>
- Gasparini, N. M., Whipple, K. X., & Bras, R. L. (2007). Predictions of steady state and transient landscape morphology using sediment-flux-dependent river incision models. *Journal of Geophysical Research*, *112*, F03S09. <https://doi.org/10.1029/2006JF000567>
- Hodge, R., Hoey, T., Maniatis, G., & Leprêtre, E. (2016). Formation and erosion of sediment cover in an experimental bedrock-alluvial channel. *Earth Surface Processes and Landforms*. <https://doi.org/10.1002/esp.3924>

- Hodge, R. A., Hoey, T. B., & Sklar, L. S. (2011). Bed load transport in bedrock rivers: The role of sediment cover in grain entrainment, translation, and deposition. *Journal of Geophysical Research*, *116*, F04028. <https://doi.org/10.1029/2011JF002032>
- Inoue, T., Izumi, N., Shimizu, Y., & Parker, G. (2014). Interaction among alluvial cover, bed roughness, and incision rate in purely bedrock and alluvial-bedrock channel. *Journal of Geophysical Research: Earth Surface*, *119*, 2123–2146. <https://doi.org/10.1002/2014JF003133>
- Johnson, J. P. (2014). A surface roughness model for predicting alluvial cover and bed load transport rate in bedrock channels. *Journal of Geophysical Research: Earth Surface*, *119*, 2147–2173. <https://doi.org/10.1002/2013JF003000>
- Johnson, J. P., & Whipple, K. X. (2007). Feedbacks between erosion and sediment transport in experimental bedrock channels. *Earth Surface Processes and Landforms: The Journal of the British Geomorphological Research Group*, *32*. <https://doi.org/10.1002/esp.1471>
- Johnson, J. P., & Whipple, K. X. (2010). Evaluating the controls of shear stress, sediment supply, alluvial cover, and channel morphology on experimental bedrock incision rate. *Journal of Geophysical Research*, *115*(F2). <https://doi.org/10.1029/2009JF001335>
- Lague, D. (2010). Reduction of long-term bedrock incision efficiency by short-term alluvial cover intermittency. *Journal of Geophysical Research*, *115*(F2). <https://doi.org/10.1029/2008JF001210>
- Lague, D. (2014). The stream power river incision model: Evidence, theory and beyond. *Earth Surface Processes and Landforms*, *39*, 38–61. <https://doi.org/10.1002/esp.3462>
- Lamb, M. P., Dietrich, W. E., & Sklar, L. S. (2008). A model for fluvial bedrock incision by impacting suspended and bed load sediment. *Journal of Geophysical Research*, *113*, F03025. <https://doi.org/10.1029/2007JF000915>
- Moreira, R. R. H. (2016). Deposits emplaced in upper regime (doctoral dissertation, University of South Carolina).
- Nittrouer, J. A. (2013). Backwater hydrodynamics and sediment transport in the lowermost Mississippi River Delta: Implications for the development of fluvial-deltaic landforms in a large lowland river. In *Deltas: landforms, ecosystems, and human activities* (Vol. 358, pp. 48–61). Gothenburg, Sweden: International Association of Hydrological Sciences Publication.
- Nittrouer, J. A., Mohrig, D., Allison, M. A., & Peyret, A. P. B. (2011). The lowermost Mississippi River: A mixed bedrock-alluvial channel. *Sedimentology*, *58*(7), 1914–1934. <https://doi.org/10.1111/j.1365-3091.2011.01245.x>
- Paola, C., Parker, G., Seal, R., Sinha, S. K., Southard, J. B., & Wilcock, P. R. (1992). Downstream fining by selective deposition in a laboratory flume. *Science-New York Then Washington*, *258*, 1757–1757.
- Parker, G. (1990). Surface-based bedload transport relation for gravel rivers. *Journal of Hydraulic Research*, *28*(4), 417–436. <https://doi.org/10.1080/00221689009499058>
- Parker, G. (1991). Selective sorting and abrasion of river gravel. I: Theory. *Journal of Hydraulic Engineering*, *117*(2), 131–147. [https://doi.org/10.1061/\(ASCE\)0733-9429\(1991\)117:2\(131\)](https://doi.org/10.1061/(ASCE)0733-9429(1991)117:2(131))
- Parker, G. (2004). 1D sediment transport morphodynamics with applications to rivers and turbidity currents. E-book available at Gary Parker's Morphodynamics Web Page, last update April, 13, 2006.
- Parker, G. (2008). Transport of gravel and sediment mixtures. *Sedimentation engineering: Processes, measurements, modeling, and practice*, *110*, 165–252. <https://doi.org/10.1061/9780784408148.ch03>
- Parker, G., & Klingeman, P. C. (1982). On why gravel bed streams are paved. *Water Resources Research*, *18*(5), 1409–1433.
- Parker, G., & Sutherland, A. J. (1990). Fluvial armor. *Journal of Hydraulic Research*, *28*(5), 529–544.
- Parker, G., & Wilcock, P. R. (1993). Sediment feed and recirculating flumes: Fundamental difference. *Journal of Hydraulic Engineering*, *119*(11), 1192–1204. [https://doi.org/10.1061/\(ASCE\)0733-9429](https://doi.org/10.1061/(ASCE)0733-9429)
- Shaw, J. B., Mohrig, D., & Whitman, S. K. (2013). The morphology and evolution of channels on the Wax Lake Delta, Louisiana, USA. *Journal of Geophysical Research: Earth Surface*, *118*, 1562–1584. <https://doi.org/10.1002/jgrf.20123>
- Singh, A., Lanzoni, S., Wilcock, P. R., & Foufoula-Georgiou, E. (2011). Multiscale statistical characterization of migrating bed forms in gravel and sand bed rivers. *Water Resources Research*, *47*, W12526. <https://doi.org/10.1029/2010WR010122>
- Sklar, L. S., & Dietrich, W. E. (2004). A mechanistic model for river incision into bedrock by saltating bed load. *Water Resources Research*, *40*, W06301. <https://doi.org/10.1029/2003WR002496>
- Sloff, K., van der Sligte, R., Huisman, Y., & Fuhrhop, H. (2012). Morphological model of the Thie-Meuse delta, KPP Rivierkunde 2021—Stabilele keringnen, Deltares, <http://www.commissiemer.nl/docs/mer/p29/p2991/2991-012morphological-model.pdf>
- Tuijinder, A. P., Ribberink, J. S., & Hulscher, S. J. (2009). An experimental study into the geometry of supply-limited dunes. *Sedimentology*, *56*(6), 1713–1727. <https://doi.org/10.1111/j.1365-3091.2009.01054.x>
- Turowski, J. M., Lague, D., & Hovius, N. (2007). Cover effect in bedrock abrasion: A new derivation and its implications for the modeling of bedrock channel morphology. *Journal of Geophysical Research*, *112*, F04006. <https://doi.org/10.1029/2006JF000697>
- Van Rijn, L. C. (1984). Sediment transport, part III: Bed forms and alluvial roughness. *Journal of hydraulic engineering*, *110*(12), 1733–1754. [https://doi.org/10.1061/\(ASCE\)0733-9429\(1984\)110:12\(1733\)](https://doi.org/10.1061/(ASCE)0733-9429(1984)110:12(1733))
- Vanoni, V. A. (1975). Sedimentation Engineering. *American Society of Civil Engineers, Manuals and Reports on Engineering Practice*, *54*, 745.
- Vanoni, V. A., & Brooks, N. H. (1957). Laboratory studies of the roughness and suspended load of alluvial streams. Sedimentation Laboratory California Institute of Technology, Pasadena, California, Report No. E-68.
- Viparelli, E., Gaeuman, D., Wilcock, P., & Parker, G. (2011). A model to predict the evolution of a gravel bed river under an imposed cyclic hydrograph and its application to the Trinity River. *Water Resources Research*, *47*, W02533. <https://doi.org/10.1029/2010WR009164>
- Viparelli, E., Lauer, J. W., Belmont, P., & Parker, G. (2013). A numerical model to develop long-term sediment budget using isotopic sediment fingerprints. *Computers and Geosciences*, *53*, 114–122. <https://doi.org/10.1016/j.cageo.2011.10.003>
- Viparelli, E., Nittrouer, J. A., & Parker, G. (2015). Modeling flow and sediment transport dynamics in the lowermost Mississippi River, Louisiana, USA, with an upstream alluvial-bedrock transition and a downstream bedrock-alluvial transition: Implications for land building using engineered diversions. *Journal of Geophysical Research: Earth Surface*, *120*, 534–563. <https://doi.org/10.1002/2014JF003257>
- Whipple, K. X. (2004). Bedrock rivers and the geomorphology of active orogens. *Annual Review of Earth and Planetary Sciences*, *32*, 151–185. <https://doi.org/10.1146/annurev.earth.32.101802.120356>
- Whipple, K. X., Hancock, G. S., & Anderson, R. S. (2000). River incision into bedrock: Mechanics and relative efficacy of plucking, abrasion, and cavitation. *Geological Society of America Bulletin*, *112*(3), 490–503. [https://doi.org/10.1130/0016-7606\(2000\)112](https://doi.org/10.1130/0016-7606(2000)112)
- Whipple, K. X., & Tucker, G. E. (2002). Implications of sediment-flux-dependent river incision models for landscape evolution. *Journal of Geophysical Research*, *107*, 2039. <https://doi.org/10.1029/2000JB000044>
- Wilcock, P. R., & Crowe, J. C. (2003). Surface-based transport model for mixed-size sediment. *Journal of Hydraulic Engineering*, *129*(2), 120–128. [https://doi.org/10.1061/\(ASCE\)0733-9429\(2003\)129:2\(120\)](https://doi.org/10.1061/(ASCE)0733-9429(2003)129:2(120))
- Wong, M., Parker, G., DeVries, P., Brown, T. M., & Burges, S. J. (2007). Experiments on dispersion of tracer stones under lower-regime plane-bed equilibrium bed load transport. *Water Resources Research*, *43*, W03440. <https://doi.org/10.1029/2006WR005172>

- Wright, S., & Parker, G. (2004). Flow resistance and suspended load in sand-bed rivers: Simplified stratification model. *Journal of Hydraulic Engineering*, 130(8), 796–805. [https://doi.org/10.1061/\(ASCE\)0733-9429\(2004\)130:8\(796\)](https://doi.org/10.1061/(ASCE)0733-9429(2004)130:8(796))
- Zhang, L., Parker, G., Stark, C. P., Inoue, T., Viparelli, E., Fu, X., & Izumi, N. (2015). Macro-roughness model of bedrock-alluvial river morphodynamics. *Earth Surface Dynamics Discussions*, 2, 297–355. <https://doi.org/10.5194/esurfd-2-297-2014>